Starch Turnover and Metabolism during Flower and Early Embryo Development

Hedhly, Afif ; Vogler, Hannes ; Schmid, Marc W ; Pazmino, Diana ; Gagliardini, Valeria ; Santelia, Diana ; Grossniklaus, Ueli

DOI: https://doi.org/10.1104/pp.16.00916

Short title:

Starch turnover during flower development

Corresponding Authors:

Ueli Grossniklaus and Afif Hedhly

Department of Plant and Microbial Biology, University of Zurich

Zollikerstrasse 107, CH-8008, Zurich, Switzerland

+41 44 634 8240, +41 44 634 8251

grossnik@botinst.uzh.ch, afif.hedhli@uzh.ch

Title:

Starch turnover and metabolism during flower and early embryo development in *Arabidopsis thaliana*

Authors

Afif Hedhly*, Hannes Vogler, Marc W. Schmid, Diana Pazmino, Valeria Gagliardini, Diana Santelia, Ueli Grossniklaus*

Department of Plant and Microbial Biology and Zürich-Basel Plant Science Center, University of Zurich, Zollikerstrasse 107, CH-8008 Zürich, Switzerland.

One Sentence Summary:

A systematic characterization of starch turnover during reproductive development unravels new starch deposits and sheds light on starch metabolism and carbohydrate transport in reproductive tissues.

Footnotes:

[1]This work was supported by the University of Zürich, an IEF Marie Curie Grant (Transepigen-254797) to A.H, an ERC Advanced Grant (MEDEA-250358) and a Research and Technology Development project from SystemsX.ch (MecanX) to U.G, and a Swiss National Science Foundation grant (SNSF 31003A_147074) to D.S.

*Address correspondence to grossnik@botinst.uzh.ch or afif.hedhli@uzh.ch

A.H. and U.G. conceived the project; A.H., D.S., and U.G. designed experiments; A.H. carried out most of the experiments, made graphical outputs, and wrote the manuscript with help from H.V.; A.H., H.V., M.W.S., and U.G. analyzed results; M.W.S. analyzed microarray data; D.P. carried out starch quantification; V.G. performed the ddPCR analysis; all authors commented on the manuscript.

ABSTRACT

The accumulation of starch within photosynthetic tissues and within dedicated storage organs has been extensively characterized in many species, and a function in buffering carbon availability or in fueling later growth phases, respectively, has been proposed. However, developmentally regulated starch turnover within heterotrophic tissues other than dedicated storage organs is poorly characterized and its function is not well understood. Here, we report on the characterization of starch turnover during flower, early embryo, and silique development in *Arabidopsis thaliana*, using a combined clearing-staining technique on whole-mount tissue. Besides the two previously documented waves of transient starch accumulation in the stamen envelope, occurring during meiosis and pollen mitosis I, we identified a novel, third wave of starch amylogenesis/amylolysis during the last stages of stamen development. To gain insights into the underlying molecular mechanisms, we analyzed publicly available microarray data, which revealed a developmentally coordinated expression of carbohydrate transport and metabolism genes during these waves of transient starch accumulation. Based on this analysis, we characterized starch dynamics in mutants affecting hexose phosphate metabolism and translocation, and identified the glucose-6-phosphate/phosphate antiporter GPT1 as the putative translocator of glucose-6-phosphate for starch biosynthesis in reproductive tissues. Based on these results, we propose a model of starch synthesis within the pollen grain, and discuss the nutrient transport route feeding the embryo within the developing seed.

INTRODUCTION

Starch is the major storage carbohydrate in plants. It exists as transitory starch or, more or less permanently, as storage starch (Streb and Zeeman, 2012). Transitory starch accumulates during the day within chloroplasts of photosynthetic tissues and is degraded during the night. In contrast, storage starch accumulates within dedicated organs where it is stored for longer periods. Transitory starch is considered an important integrator of plant growth, buffering recurrent changes in carbon availability that result from the diurnal light-dark rhythm (Geigenberger, 2011; Streb and Zeeman, 2012). Storage starch covers long-term carbon needs, fueling germination or regrowth after certain dormancy periods (Smith, 2012). However, throughout plant development other types of starch, which do not necessarily fall into these broad categories, accumulate within cells of sink tissues, such as most reproductive tissues. Various waves of amylogenesis/amylolysis have been reported during flower and seed development in different species. The best-characterized waves of transient starch accumulation are those taking place during stamen and pollen development. One to two cycles of starch amylogenesis/amylolysis occur either in the sporogenous cells or the anther wall layers (Feijó and Pais, 1988; Clément and Pacini, 2001). Much less is known about starch dynamics during carpel and embryo development. The only systematic characterization of starch turnover during fruit and seed development was done more than a half century ago in *Dianthus chinensis* (Buell, 1952). Recently, starch dynamics during seed development in *Brassica napus* and Arabidopsis, both of which accumulate oils in their mature seeds, have been characterized (Baud et al., 2002; Andriotis et al., 2010a). However, the developmental and physiological significance of this starch accumulation is not well understood.

Despite the importance of starch turnover for plant development and agriculture, the molecular mechanisms underlying starch metabolism are still not completely resolved. A fully chloroplast-based biosynthesis using photosynthetic metabolites is the widely accepted pathway in mesophyll cells (Streb and Zeeman, 2012). Three plastidic enzymes convert the Calvin-Benson cycle-derived fructose-6-phosphate (Fru6P) to ADP-glucose (ADPGlc). The phosphoglucose isomerase (PGI) converts Fru6P to glucose-6-phosphate (Glc6P); then Glc6P is converted to Glc1P by phosphoglucomutase (PGM); Glc1P is then metabolized to ADPGlc by the ADPGlc pyrophosphorylase (AGPase). There is, however, an ongoing discussion over the origin of the residual starch (3-15%) in some null mutants of the plastidic PGI-PGM-AGPase pathway (Niewiadomski et al., 2005; Kunz et al., 2010; Streb et al., 2009; Bahaji et al., 2015), the significance of the observed uptake of exogenously applied glucose-1-phosphate (Glc1P) to isolated chloroplast and its conversion to starch (Fettke et al., 2011), the disputed possibility of an alternative cytosolic route of ADPGlc synthesis by sucrose synthase (SUS) and its potential translocation to the chloroplast (Muñoz et al., 2005; Barrat et al., 2009; Baroja-Fernández et al., 2012; Smith et al., 2012), and the recently suggested PGI1-independent starch synthesis (Bahaji et al., 2015). Starch synthesis in non-photosynthetic plastids relies on the translocation of carbon from the cytosol, mainly in the form of hexose phosphate (Flügge, 1999). Accumulating evidence in all

dicotyledonous plant species studied so far (e.g. Arabidopsis, *Vicia faba*, potato) points to Glc6P as the preferred translocated hexose-phosphate, and the glucose-6-phosphate/phosphate antiporter GPT1 as the active translocator (Kammerer et al., 1998; Geigenberger et al., 2004; Niewiadomski et al., 2005; Rolletschek et al., 2007; Zhang et al., 2008). This is further supported by the fact that loss of plastidial PGI1 activity impacts starch accumulation only in autotrophic Arabidopsis cells (Yu et al., 2000; Tsai et al., 2009), while mutations affecting plastidial PGM1 result in a low starch phenotype both in autotrophic and heterotrophic tissues (Caspar et al., 1985). Starchless amyloplasts were reported in *gpt1* mutant pollen grains, and a dual function of GPT1 in starch synthesis and the oxidative pentose phosphate pathway (OPPP) was suggested (Kammerer et al., 1998; Niewiadomski et al., 2005; Kunz et al., 2010). However, a seed-specific knock-down of GPT1 activity revealed that starch grains still accumulated in arrested embryos (Andriotis et al., 2010b*)*. Thus, it is still unclear whether starch metabolism in heterotrophic cells of Arabidopsis is based on GPT1-mediated Glc6P translocation. Arabidopsis does not accumulate starch in its mature seeds; hence, seeds are not the best system to characterize long-term storage starch. However, given the extensive molecular knowledge in this species and the good understanding of transitory starch metabolism in its leaves, Arabidopsis is an excellent system to characterize developmentally regulated starch accumulation.

Here, we characterized starch dynamics throughout flower development as well as early embryo and silique development in Arabidopsis, using a combined clearing-staining technique on whole-mount tissues (Herr, 1972). We analyzed publicly available microarray data of different stages and organs of flowers and seeds, and related the transcriptional dynamics to the observed starch turnover in the flower and young embryo. This analysis indicated that GPT1 may be the translocator of hexose phosphate for starch biosynthesis in heterotrophic tissues. An analysis of starch dynamics in *gpt1, pgi1*, and *pgm1* mutants, which are related to Glc6P transport and metabolism, provided evidence for the role of *GPT1* in this process. Our work provides new insight into starch synthesis in the pollen grain and the nutrient transport route feeding the embryo during seed development. Understanding starch dynamics and metabolism during sexual reproduction is an important step towards a better understanding of the function of developmentally regulated starch metabolism.

RESULTS

A Previously Undescribed, third Starch Synthesis Wave Occurs in Stamen just before Anthesis

Using iodine staining, we could observe a single wave of starch accumulation/degradation in sporogenous and gametophytic cells, and three waves within the sporophytic anther wall layers. The developmental delay of short stamens with respect to long stamens was critically helpful in tracking the highly dynamic starch turnover, especially in revealing the existence of a third wave in the staminal envelope.

During early flower development, starch accumulated mainly in the peduncle and the receptacle (Figure 1A). As soon as the flower organ primordia developed, starch accumulated to high amounts in their basal parts (Figure 1, B-D). Paralleling the development of the stamen filament and the connective tissue of the anther, amylogenesis extended to these two tissues (Figure 1E). At the completion of anther wall layer formation, starch accumulation extended beyond the filament and the connective tissue into the newly differentiated endothecium (Figure 1F). Starch accumulation reached its first maximum in the stamen at the tetrad stage (Figure 1, G, H and I). Interestingly, concomitant with the release of the microspores from the tetrad, starch practically vanished from the stamens (Figure 1J).

As microspore development proceeded to pollen mitosis I (PM I), a new wave of starch accumulation occurred in the sporophytic tissues of the stamen (Figure 1, J-M). During or just after PM I, while starch deposits started to build up in the bicellular pollen grain, a concomitant increase in starch accumulation occurred in the staminal envelope, reaching a second amylogenesis peak that was higher than that of the first wave (Figure 1, L and M). Soon thereafter, encompassing pollen mitosis II (PM II), starch accumulation in the pollen grain reached its maximum, while drastic amylolysis occurred in the anther wall layers (Figure 1, N and O).

Shortly after the amylogenesis peak in the pollen grain, prominent starch deposition was observed in all sporophytic tissues of the stamen (Figure 1, P, Q, V and W). Compared to the previous two staminal envelope waves, this wave showed the strongest starch accumulation. Then, just before the final extension of the stamen to the level of the stigma, starch deposits completely vanished from the anther (except stomata), while conspicuous deposits accumulated in the filament (Figure 1, T, X and Y). Very few, small starch grains could be seen in maturing pollen grains (Figure 1X). The remaining starch deposits in the filament were largely consumed by the time the stamen reached the stigma and the flower opened (Figure 1U).

Starch Accumulates in Proliferating Tissues during Early Zygote and Embryo Development

In contrast to the staminal envelope, starch metabolism followed sequential amylogenesis and amylolysis in different tissues of the carpel/silique, ovule, and embryo.

Starch accumulated first in the lateral walls of young carpels (Figure 1, D and E). Concomitant with the development of ovule primordia, starch deposits appeared in the placenta-septum region at the basal part of ovule primordia, and were progressively lost from the lateral carpel wall (Figure 1, G and I). During meiosis, more prominent starch accumulation occurred in the placenta-funiculus region and in the distal funiculus joining the chalaza (Figure 2, A-C). These accumulations extended to the integuments surrounding the developing female gametophyte (Figure 2D). During the last stages of flower development, while the progressive depletion of starch was observed in the placenta-septum region, conspicuous starch deposition occurred both in the style (Figure 2E, also compare Figure 1, T and U) and the ovule. The largest deposits in the ovule were seen in the central cell, where starch accumulation started before the fusion of the two polar nuclei (Figure 2F) and further increased after the formation of the secondary endosperm nucleus (Figure 2G). However,

also the egg cell, the distal part of the funiculus, the chalazal proliferating tissue, and the micropylar part of the inner and outer integuments had starch deposits.

During the progamic phase (i.e. the period from pollination to fertilization), the conspicuous starch deposits in the ovule were maintained (Figure 2H). However, while starch gradually disappeared from the micropylar integuments after fertilization, it was maintained in both the uni-nuclear endosperm and the zygote (Figure 2I). Starch persisted in the apical cell after the division of the zygote (single-cell stage of the embryo proper), and in the endosperm until approximately the eight-nuclear stage (Figure 2, J-M). Interestingly, starch was gradually consumed in the endosperm along the micropylar-chalazal axis (Figure 2L). Concomitant with the cellular and nuclear divisions of zygote and endosperm, respectively, starch gradually built up in the proliferating tissues of the ovule (Figure 2, L and M). At the single-cell stage of the embryo proper, the only conspicuous starch deposits in the seed were seen as a ring-like structure in the sporophytic tissues of the ovule at the chalazal pole of the embryo sac (Figure 2N). While the tightly packed and stretched cells in the center of this region had barely any starch, peripherally located cells accumulated a high quantity (Figure 2, O and P). The micropylar-most cells of this structure had an inverted cup-like shape and were in direct contact with the chalazal cyst of the endosperm. At the octant embryo stage, the whole seed coat accumulated starch in all layers, with even stronger staining detected at the dermatogen stage (Figure 2, Q and R). Interestingly, the ovary wall, the placenta-septum region, and the funiculus showed a gradual basipetal starch accumulation paralleling that of seed development (Figure 2, S, V and W).

In Silico Analysis of Sugar- and Starch-related Gene Expression Profiles during Flower Development

To check whether this highly dynamic starch turnover pattern is related to transcriptional activities of carbohydrate transport and metabolism genes, we analyzed publicly available microarray data from flower and silique tissues at different developmental stages. Based on the microscopic characterization of flower and early seed development, and to cover a wide variety of reproductive tissues, we chose to focus our analyses on two developmental processes: (i) pollen development from the microspore stage to maturation (haploid male gametophyte), and (ii) the chalazal seed coat (diploid maternal tissue) and chalazal endosperm (fertilization product) regions of the developing seed.

In developing pollen, we could distinguish three well-defined gene expression clusters (Figure 3, and Supplemental Fig. S1). The first cluster (Figure 3) was characterized by high transcription during early microspore development, peaking in uni-nucleate or bicellular pollen, followed by a sharp or gradual decrease during later stages of development. This corresponds to the stage when we observed the unique starch amylogenesis wave in the developing pollen grain. Most of the genes for starch metabolism as well as the *GPT1* gene encoding a translocator belong to this cluster (see Table 1 for the full names of the genes). Interestingly, the gene coding for the AGPase regulatory subunit APL2, typical of mesophyll cells, was the only APL isoform present in this cluster. All three

expressed starch synthase genes (*SS1*, *SS3*, and *SS4*) also belong to this cluster. Except for the genes encoding the glucan water dikinase GWD1 and the β-amylases BAM1, BAM4, and BAM9, most of the genes within the degradation pathway were also in the first cluster.

Microscopic analyses revealed high starch accumulation in the chalazal seed coat throughout early seed development (Figure 2, M-R). Paralleling this pattern, we identified significant expression of genes for starch metabolism (Figure 4, B and C) and *GPT1* (Figure 4D). Strikingly, neither *PGM1* nor any *APL* isoforms of the biosynthetic pathway were significantly expressed above threshold. In contrast to the situation in the pollen grain, starch degradation pathway genes showed a high expression level, including the starch glucan phosphatase gene *SEX4*, the genes encoding the catalytic plastidial and cytosolic isoforms BAM1 and BAM5, respectively, and the uncharacterized *BAM9* gene. The absence of any significant expression of many starch metabolism genes in the chalazal endosperm is congruent with our finding that no starch accumulated in this region. Comparing the expression level of sugar metabolism and transport genes in different tissues of the seed (Figure 4E, Supplemental Figure S3 and S4), the chalazal region (seed coat and endosperm, Figure 4E) showed the highest expression of invertase and sugar transporter genes during early embryo development.

Down-Regulation of *GPT1* Expression Induces Tissue-specific Deregulation of Starch Biosynthesis

Given the intriguing expression pattern of *GPT1*, we investigated whether GPT1 is indeed the translocator of Glc6P for starch biosynthesis in reproductive tissues. To do so, we analyzed starch dynamics in three mutants potentially affecting the plastidial Glc6P content: the homozygous *pgi1-1*, *pgm1-1*, and *gpt1-3* mutants (highlighted with red boxes in Figure 7). In *pgm1-1* homozygotes, starch was undetectable both in photosynthetic and reproductive tissues, including inflorescence stalks and flower peduncles (Figure 5, E, F, J1-J3, N, and T1-T3). In contrast, most inflorescences of *pgi1-1* homozygotes showed starch dynamics comparable to the wild type in all reproductive tissues except for the sepals where an appreciable reduction was observed (Figure 5, C, D, I1-I3, M, and S1-S3). In some inflorescences, even higher starch accumulation was observed than in the wild type (compare Figures 5B and 5D). Compared to *pgm1-1*, a slightly higher residual starch accumulation was observed in mesophyll cells of *pgi1-1* cauline leaves, and much higher starch accumulation was seen lining the vascular bundles (compare Figures 5C and 5E). Mutations affecting *GPT1* were reported to be embryo lethal; however, there are alleles available as homozygous insertion lines (*gpt1-3*, *gpt1-5*, and *gpt1-6*), which did not reduce *GPT1* transcription and had thus not been physiologically characterized (Niewiadomski et al., 2005). Our analysis of starch turnover within *gpt1-3* homozygotes revealed a reduction in starch accumulation in the carpel and during early silique development. Compared to the wild type, while lower starch accumulation was observed during early stages of flower development (Figure 5H), starch dynamics during stamen development appeared unaffected (Figure 5, K1, K2 and O). At anthesis and during the early stages of silique and seed development, a strong reduction in starch accumulation was observed in

the pistil (Figure 5O) and the ovule (Figure 5Q). The conspicuous starch accumulation usually seen in the central cell of wild-type ovules (Figure 5P and R1) was either strongly reduced (Figure 5R2) or absent in the *gpt1-3* mutant (Figure 5R3). After fertilization, starch accumulation was also affected in young seeds (Figure 5R4), the style, and the silique valve (Figure 5R5). Starch amylogenesis in the seed after the octant embryo stage appeared unaffected (Figure 5R5).

To check whether *GPT1* transcript level was affected in an organ-specific manner in *gpt1-3* homozygotes, we quantified the concentration of *GPT1* mRNA using the highly sensitive droplet digital PCR (ddPCR) method using RNA isolated from sepals, stamens, and carpels. Compared to the wild type, mutant carpels showed a highly significant reduction in *GPT1* transcript levels at anthesis (Figure 6A), correlating with the impact of the mutation on starch accumulation in the carpel. The enzymatic quantification of starch content also revealed a slight but non-significant reduction in all organs ($p > 0.05$, Figure 6B).

DISCUSSION

Starch Turnover during Flower and Early Silique Development is Highly Dynamic

In many plant species characterized so far, a single wave of conspicuous starch accumulation is usually observed during microgametogenesis, while one to two amylogenesis/amylolysis waves are commonly observed in the staminal envelope (reviewed in Clément and Pacini, 2001). These starch waves were suggested to sustain growth and differentiation of the anther wall layers, to translocate nutrients to the highly active tapetum and to the loculus, to provide carbon skeletons for the formation of lipid droplets within the pollen grain, and to store excess food during the anther maturation phase (Reznickova and Willemse, 1980; Miki-Hirosige and Nakamura, 1983; Pacini and Franchi, 1983; Clément et al., 1994; Clément and Pacini, 2001). In this work, apart from confirming the occurrence of these waves in *Arabidopsis thaliana*, we unraveled the existence of a third wave of starch amylogenesis/amylolysis in the staminal envelope just before anthesis. Its occurrence close to anthesis suggests that products of starch degradation may sustain final maturation, elongation of the filaments to reach the level of the stigma, dehiscence, and/or other functions yet to be discovered. Whether the presence of this third wave is specific to Arabidopsis, species producing tricellular pollen grains or, more generally, species with filament elongation prior to anthesis deserves further investigations.

During carpel development before anthesis, rather than a strict wave in a given tissue, starch accumulated sequentially in different tissues and organs, such as the lateral carpel walls in young carpels, the placenta-septum and funiculus-chalaza regions during early ovule development, and, especially, the parenchymatic tissue of the style and the central cell at flower opening. These starch deposits may buffer the growth and development not only of reproductive cells but also of the sporophytic tissues that are growing and maturing at the same time (Buell, 1952). After pollination, while starch vanished progressively from the integuments, the embryo, and the endosperm, conspicuous starch deposits built up in the proliferating tissues of ovule, which, at the one-cell stage

of the embryo proper, had the only conspicuous starch deposits in the seed, forming a ring-like structure surrounding the chalazal cyst. This chalazal proliferating tissue, which has an inverted cup-like shape, lies between the terminus of the vascular strand and the chalazal end of the embryo sac, and has a high metabolic activity in the closely related species *Capsella bursa-pastoris* (Schulz and Jensen, 1971). Moreover, the elongating embryo sac, while crushing nucellar cells during its growth towards this proliferating tissue, develops ingrowths to absorb nutrients from these tissues. Soon after, the chalazal cyst of the endosperm develops a haustorial base that penetrates into the proliferating tissue (Nguyen et al., 2000). Taken together, although the integuments might ensure some nutrient flux to the growing zygote/embryo (Schulz and Jensen, 1969; Mansfield and Briarty, 1991), the following observations suggest a different nutrient transport route for endosperm and embryo: (i) the extensive starch deposits surrounding the chalazal cyst, (ii) the high transfer activity characterizing the chalazal end of the embryo sac, (iii) the absence of a membrane system during the syncytial phase of endosperm development, and (iv) the gradual micropylar-chalazal starch consumption in the endosperm all indicate that assimilates are transported along the following pathway: vascular tissue > proliferating tissue > endosperm > embryo. Although starch accumulation *per se* does not represent a carbohydrate translocation process, correlations in starch turnover between adjacent tissues or specific patterns of starch accumulation suggest potential starch degradation, sugar translocation, and nutrient transport processes (Buell, 1952).

The analysis of starch dynamics in three homozygous mutants affecting Glc6P metabolism or transport identified GPT1 as the likely translocator related to starch biosynthesis in heterotrophic floral tissues. While all reproductive tissues were starchless in *pgm1-1*, no major effects on starch dynamics were reported for *pgi1-1*. Only sepals showed an appreciable reduction in starch accumulation in *pgi1-1*, suggesting that sepals have a starch metabolism pathway similar to that of leaf mesophyll cells. Although mutations in *GPT1* were documented to be embryo lethal, we found that a homozygous viable allele showed reduced starch accumulation during early flower development, and an effect on starch dynamics in female tissues during anthesis and early embryo/silique development. In particular, starch accumulation in the central cell was absent in *gpt1-3* mutants. Indeed, *GPT1* transcript levels were significantly reduced at anthesis in mutant carpels compared to stamens and sepals. Although these results show that *GPT1* plays an important role in the starch metabolism of reproductive tissues, the unaffected starch dynamics in stamen indicates either a tissue-specific effect of the T-DNA insertion on the regulation of *GTP1* or the existence of an alternative pathway for hexose phosphate transport in this organ.

In silico Analyses of Gene Expression at Specific Reproductive Stages with High Starch Turnover Unravel Potential Carbohydrate Metabolic Pathways

Developing microspores and growing pollen tubes are symplastically isolated, and sugar transport to these heterotrophic organisms occurs mainly via the apoplast from the locular fluid of the stamen and the extracellular matrix of the pistilar transmitting tissue, respectively. The analysis of gene expression related to sugar, hexose-phosphate, and starch metabolism during pollen

development revealed highly coordinated gene expression, with three clusters of transcriptional activities. The first cluster, which includes most of the genes for starch synthesis and degradation, characterized the early stages of microspore development and coincided with the starch wave during microgametogenesis. This transcriptional co-regulation of the three processes suggests that sugar and hexose-phosphate transport and metabolism genes expressed during this stage might be related to starch metabolism. They also suggest that starch synthesis/degradation transcriptional activities are not discrete and temporally separated metabolic pathways, in agreement with similar findings during seed development (Andriotis et al., 2010a). Based on these transcriptional patterns, and the GPT1-mediated hexose-phosphate transport to amyloplasts for starch biosynthesis, a model of sugar-starch metabolism is proposed for the starch wave occurring during microspore development (Figure 7, yellow path). Sucrose could be metabolized in the apoplast by cwINV4, and monosaccharides, either derived from invertase activity or the locular fluid, are likely transported by the highly expressed STP2 and SWEET8 transporters, the latter a member of the SUGARS WILL EVENTUALLY BE EXPORTED TRANSPORTER family. While STP2 was suggested to have a role in Glc uptake (Truernit et al., 1999), the plasma membrane sugar transporter SWEET8, which showed the highest expression level, has been shown to mediate at least Glc transport (Chen et al., 2010). The *rpg1* mutant disrupting *SWEET8* revealed its importance for cell integrity and exine pattern formation (Guan et al., 2008) but whether it fulfills an uptake activity is unknown. Within the cytosol, the expression of two isoforms derived from each of the *SPS* and *SPP* genes suggests high sucrose biosynthetic activities paralleling starch biosynthesis. *SUS* gene expression levels remained unaltered during all stages of pollen development and *in vitro* pollen tube growth, pointing toward SUS-independent starch biosynthesis, a finding that contrasts with SUS-based starch biosynthesis suggested for other tissues (Déjardin et al., 1997; Angeles-Núñez and Tiessen, 2010). Low *SUS* and high invertase expression levels imply a higher abundance of Glc and Fru compared to UDPGlc. Based on this observation, hexokinases and cytoplasmic PGI would play an important role in the pathway producing Fru6P and Glu6P (Figure 7); Glc6P is then translocated to plastids by GPT1.

Comparing starch synthesis and degradation between different reproductive tissues and organs revealed a variation in the presence/absence or in the specific expressed isoform for the step-limiting AGPase (whether it is based on autotrophic or heterotrophic APL subunits), starch synthase, glucan phosphorylating/dephosphorylating, and exo-amylase genes. While the prevalence of the specific autotrophic or heterotrophic APL regulatory subunit might reflect distinct regulatory starch biosynthesis needs in different tissues (Crevillén et al., 2003; Crevillén et al., 2005), the variation in the expressed isoforms for the starch synthase, and of some members within the degradation pathway, suggests that the different starch deposits might be structurally distinct.

Starch turnover during early seed development suggests an important role for the vascular tissue > chalazal proliferating tissue > chalazal endosperm > embryo nutrient transport route to nourish endosperm and embryo, at least during early seed development. A comparison of transcriptional activities within different territories of the seed reinforces this view. While globally similar

transcriptional activities in the three regions of the endosperm can be appreciated, the highest expression levels of cell wall and cytoplasmic invertases occur in the chalazal seed coat and the chalazal endosperm, respectively (Figure 6, Supplemental Figure S3). But the high expression level of so far uncharacterized genes of the SWEET and EARLY RESPONSIVE TO DEHYDRATION6-LIKE (ERDL) families, either at the whole seed level or within the chalazal region, adds a challenging layer of complexity to traditionally simplified models (Fallahi et al., 2008; Wang and Ruan, 2012; Baud et al., 2002). Knowledge about the substrate specificities, subcellular localization, and function of the members of these families would certainly improve these models.

Our systematic microscopic and transcriptomic analyses of starch and sugar metabolism during flower and early silique development sets the foundation for further research on metabolic pathways, using more specific microscopical and molecular approaches, in particular organ-, tissue-, or cell-specific transcriptomic and gene silencing techniques (e.g. Andriotis et al., 2010b; Schmid et al., 2015). However, the simple, effective, and quantitative microscopic technique used here will help to distinguish between models by analyzing mutants, either for genes already known to be essential for sugar and starch metabolism or, to circumvent genetic redundancy, for multiple mutants representing co-expressed genes in specific pathways.

MATERIALS AND METHODS

Plant Material, Growth Conditions, and Sampling

Arabidopsis thaliana (L.) Heynh. var. Columbia-0 (Col-0) plants, and homozygous lines for the mutants *pgm1-1*, *pgi1-1*, and *gpt1-3* were used to characterize starch turnover during flower and early silique development, for quantifying starch content, and for transcript level analyses. Both wild-type and mutant Arabidopsis seedlings were grown on MS plates for 8 days, transferred to ED73 soil (Einheitserde, Schopfheim, Germany), and grown under 16 h light and 8 h darkness at 21ºC and 18ºC, respectively. The homozygosity of insertions was confirmed using the oligonucleotide primers listed in Table S1. To increase the homogeneity between samples, 40 plants with the first flower opening on the same day were selected, the primary inflorescence of ten randomly selected plants was fixed toward the end of the light phase (after approximately 10 hours of light) on that day, and ten additional primary inflorescences each were fixed on the subsequent three days at the same time.

Histological Detection of Starch

To be able to make a systematic analysis of starch turnover during all flower stages and the early phase of silique development, we used a recipe developed by Herr (1972), which combines his 4½ clearing solution (Herr, 1971) with lugol (lactic acid:chloral hydrate:phenol:clove oil:xylene:I2:KI, 2:2:2:2:1:0.1:0.5 w:w). Inflorescences from at least 10 plants were fixed either in Carnoy fixative (ethanol:acetic acid, 3:1 v:v) or in FPA50 (Formalin:Propionic Acid:Ethanol (55%), 5:5:90 v:v) for 24 h and then moved to 70% ethanol and stored at 4ºC. The experiment was repeated three times. While Carnoy-fixed samples were ideal for tracking starch turnover, allowing much stronger starch staining, FPA50 fixed-samples were used whenever higher structural details were needed at the expense of a lower starch staining sensitivity. Individual flower buds were dissected on the slide under the stereomicroscope within a minimal amount of

70% ethanol, taking care to avoid drying out of the sample and removing sepals and petals. Excess alcohol was absorbed with a blotting paper and 20-30 μl clearing-staining solution were added before placing the cover slip and gently squashing it. Periodic acid-Schiff (PAS) staining of insoluble polysaccharide was done as previously described (Weigel and Glazebrook, 2002). For a more precise tracking of microspore developmental stages in relation to starch dynamics, one to two stamens of selected flowers where separately stained with 4′,6-diamidino-2-phenylindole (DAPI) (following Park et al., 1998, data not shown). Microscopic observations were made using Differential Interference Contrast on either a Leica DMR or a Leica DM6000 microscope (Leica Microsystems, Bensheim, Germany), and images were captured with a digital camera [Magnafire S99802 (Optronics, Muskogee, OK**,** USA) or a Leica DFC450 (Leica Microsystems, Bensheim, Germany)]. Pictures were minimally and homogeneously processed in Adobe Photoshop Lightroom 6 (Adobe Systems, San Jose, CA, USA).

Microarray Data Analysis

To gain more insights into dynamic starch turnover, we analyzed the transcriptional dynamics of genes known to be related to carbohydrate transport and metabolism using publicly available microarray data (Belmonte et al., 2013; Boavida et al., 2011; Borges et al., 2008; Honys and Twell, 2004; Kram et al., 2009; Pina et al., 2005; Qin et al., 2009; Schmid et al., 2005; Schmidt et al., 2011; Wang et al., 2008; Wuest et al., 2010; Yu et al., 2005). We curated five sets of microarrays comprising a variety of reproductive tissues and cell types at different stages: (i) specific cell types of germline lineages; (ii) individual organs of the flower before fertilization; (iii) flowers, pistils, siliques, and seeds; (iv) various developmental stages of pollen, (v) ovules before fertilization, as well as several developmental stages of (vi) embryo, (vi) endosperm, (vii) seed coat, and (viii) whole seeds (Supplementary Table S1). For each set, arrays were RMA-normalized (Irizarry et al., 2003), using an updated annotation of the ATH1 microarray (brainarray.mbni.med.umich.edu, TAIRG, version 14). We defined genes with a log2 transformed expression value above 5 in a given tissue to be expressed. For a given plot, we removed genes that were (i) not expressed in any of the tissues shown, or (ii) stably expressed at a low level (defined as an average expression level below 5 and a coefficient of variation below 0.15). We first analyzed candidate genes known to be active in sugar metabolism and transport within autotrophic source tissues and all their family members, as well as the SUC gene family for sucrose transport. Tracking the metabolic pathway, we then analyzed candidate gene families for the conversion of Glc, Fru, and UDPGlc to the different cytosolic hexose phosphate forms, and for the translocation of Glc6P into plastids. Finally, we examined genes implicated in starch synthesis and degradation, and in the transport and metabolism of degradation products within the cytoplasm (Supplementary Table S1).

Digital Droplet PCR

All sepals, stamens, and carpels were harvested separately from two flowers per plant (stage 12-13 with flowers where petals were longer than sepals and just opened flowers; Smyth et al., 1990) from a total of 36 plants (6 plants for each of the 3 biological replicates of Col-0 and *gpt1-3*). Flowers were all chosen from positions corresponding to the first 10 flowers of the first inflorescence (avoiding the first two flowers), and each individual organ was swiftly dissected under a stereomicroscope and immediately placed in a liquid N_2-cooled Eppendorf tube and stored at -80ºC. Total RNA was extracted using a NucleoSpin RNA plant kit (Macherey-Nagel, Düren, Germany) according to the manufacturer's instructions. RNA concentration and purity were determined using a Nanodrop ND-1000

spectrophotometer (Thermo Scientific, Wilmington, DE, USA). 350 ng of total RNA was used for cDNA synthesis using the Superscript II/oligo (dT) Reverse Transcriptase kit (Invitrogen, Carlsbad, CA, USA) according to the manufacturer's instructions. ddPCR assay using QX200™ Droplet Digital™ PCR System (Bio-Rad, Hercules, CA, USA) was performed according to the manufacturer's instructions. Different reference genes (*ACTIN2*, *UBC9*, *UBC21*, *PP2A,* and *IPP2*) were assayed using both regular semi-quantitative RT-PCR and ddPCR, and the *IPP2* gene was chosen as the ideal reference gene (primers and amplicon lengths are given in Table S1). Similar results were obtained using *PP2A* as a reference gene (data not shown). PCR reactions (25 μl) were prepared with 1x EvaGreen® ddPCR Supermix (Bio-Rad, Hercules, CA, USA), primers at a final concentration of 100 nM, and 5 μl of cDNA. Droplets where generated according to manufacturer's recommendation. PCR reactions were amplified under the following conditions: 95°C 5 min, 40 cycles of 96°C 30s and 60°C for 60s; followed by 4°C for 5 min, 90°C for 5 min, and held at 4°C until processing. PCR amplified droplets were read individually with the QX200 droplet reader and the result analyzed with QuantaSoft software, Version 1.4 (Bio-Rad, Hercules, CA, USA).

Starch Quantification

To quantify the starch content in the three flower organs assayed by ddPCR, a similar separate flower organ sampling procedure was used; we sampled 4 biological replicates for each line with 10 flowers per replicate. Sepals, stamens, and carpels were harvested into liquid N_2, and extracted in 200 μl of 0.7 M perchloric acid as described (Hostettler et al., 2011). Starch in the insoluble fraction was resuspended in 195 μl 0.22 M sodium acetate, pH 4.8, and determined by measuring the amount of Glc released by treatment with α-amylase (Roche, Basel, Switzerland) and amyloglucosidase (Roche, Basel, Switzerland) as described (Hostettler et al., 2011).

Supplemental Data

The following materials are available in the online version of this article.

Supplemental Figure S1. Expression values (log2-scale) for carbohydrate transport and metabolism genes during pollen development.

Supplemental Figure S2. Expression values (log2-scale) for hexose phosphate and starch metabolism genes during the development of different flower and silique organs/tissues/cells (Figures S2.1-S2.6)

Supplemental Figure S3. Full list of sugar and sugar phosphate transport and metabolism genes expressed in the chalazal region of the seed.

Supplemental Figure S4. Expression values (log2-scale) for sugar transport and metabolism gene during the development of different flower and silique organs/tissues/cells (Figures S3.1-S3.6)

Supplemental Table S1. List of the carbohydrate metabolism and transport genes included in this study. A, Sugar genes. B, Hexose phosphate and starch genes. C, Array sets. D, Primers used in this study. E, Literature cited

ACKNOWLEDGMENTS

We thank Arianna Nigro for providing homozygous *gpt1-3* seeds, and Arturo Bolaños, Christoph Eichenberger, Daniela Guthörl, and Peter Kopf for general lab support.

Table 1. List of the carbohydrate metabolism and transport genes included in the main text. Please refer to Supplemental Table S1 for a full list of all analyzed genes and the corresponding references.

Metabolic/Transport Group	Gene name	Enzyme	Locus
Sucrose synthesis	SPS1F	Sucrose Phosphate Synthase 1F	At5g20280
	SPS3F	Sucrose Phosphate Synthase 3F	At1g04920
	SPP1	Sucrose Phosphatase 1	At1g51420
	SPP2	Sucrose Phosphatase 2	At2g35840
Cell wall acid invertases	AtcwINV3	Cell Wall Invertase 3	At1g55120
	AtcwINV4	Cell Wall Invertase 4	At2g36190
Cytoplasmic neutral invertases	A/N-INVI	Alkaline/neutral Invertase I (CINV2)	At4g09510
	A/N-INVB	Alkaline/neutral Invertase B	At4g34860
	A/N-INVF	Alkaline/neutral Invertase F	At1g72000
Sugar Transport Protein	AtSTP2	Monosaccharide-H+ symporter	At1g07340
	AtSTP8	Monosaccharide-H+ symporter	At5g26250
	AtSTP14	Monosaccharide-H+ symporter	At1g77210
Vacuolar glucose transporters-like	AtVGT2	Tonoplast sugar transport protein	At5g17010
	AtVGTL	Tonoplast sugar transport protein	At5g59250
Tonoplast Monosacharide transporters	AtTMT3	Tonoplast monosaccharide transporter	At3g51490
Plastidic sugar transporters	pGlcT	Putative monosaccharide transporter	At5g16150
	MEX1	Maltose Excess 1	At5g17520
SWEET sugar transporters	SWEET4	Sugars Will Eventually be Exported Transporter 4	At3g28007
	SWEET8 (RPG1)	Sugars Will Eventually be Exported Transporter 8	At5g40260
	SWEET10	Sugars Will Eventually be Exported Transporter 10	At5g50790
Early Responsive to Dehydration6-Like	AtERDL8	Putative sugar transport protein (ERD-group)	At3g05150
	AtERDL14	Putative sugar transport protein (ERD-group)	At4g04760
Starch biosynthesis	PGI1 (PGI)	Phosphoglucoisomerase	At4g24620
	PGM1 (PGM)	Phosphoglucomutase	At5g51820
	APS1 (ADG1)	AGPase small subunit 1	At5g48300
	APL2	AGPase large subunit 2	At1g27680
	GBS1	Granule-bound starch synthase 1	At1g32900
	SS1	Soluble starch synthase 1	At5g24300
	SS2	Soluble starch synthase 2	At3g01180
	SS3	Soluble starch synthase 3	At1g11720
	SS4	Soluble starch synthase 4	At4g18240
	BE2	Starch branching enzyme 2	At5g03650
	BE3	Starch branching enzyme 3	At2g36390
	ISA1	Isoamylase 1	At2g39930
	ISA2	Isoamylase 2	At1g03310
Starch Breakdown	GWD1 (SEX1)	Glucan, water dikinase 1	At1g10760
	GWD2	Glucan, water dikinase 2	At4g24450
	PWD (GWD3)	Phosphoglucan, water dikinase	At5g26570
	SEX4	Starch excess 4	At3g52180
	BAM1 (BMY7/TR-BYM)	beta-Amylase 1	At3g23920
	BAM2 (BMY9)	beta-Amylase 2	At4g00490
	BAM5 (BMY1/RAM1)	beta-Amylase 5	At4g15210
	BAM8	beta-Amylase 8	At5g45300
	BAM9 (BMY3)	beta-Amylase 9	At5g18670
	AMY1	alpha-Amylase 1	At4g25000
	ISA3	Isoamylase 3	At4g09020
	LDA (PU1)	Limit dextrinase	At5g04360
	PHS1	Glucan phosphorylase	At3g29320
	PHS2	Glucan phosphorylase	At3g46970
	DPE1	Disproportionating enzyme	At5g64860
	DPE2	Maltose transglucosidase	At2g40840
Cytoplasmic hexose-phosphate metabolism	PGIC	Phosphoglucoisomerase	At5g42740
	PGM2	Phosphoglucomutase 2	At170730
	PGM3	Phosphoglucomutase 3	At1g23190
	HXK1	Hexokinase 1	At4g29130
	HXK2	Hexokinase 2	At2g19860
	HKL3	Hexokinase-like3	At4g37840
	AtTPS7	T6P Synthase	At1g06410
	AtTPS11	T6P Synthase	At2g18700
	AtTRE1	Trehalase1	At4g24040
Plastidic translocators and translocator-likes	AtGPT1	6-phosphate/phosphate translocator 1	At5g54800
	AtGPT-like	glucose 6 phosphate/phosphate translocator-like protein	At5g17630
	TPT (TPT1)	phosphate/triose-phosphate translocator precursor	At5g46110

FIGURE LEGENDS

Figure 1. The three starch synthesis waves in the stamen envelope. A-J first wave, J-O second wave, and P-Z third wave. A, Starch accumulates within the peduncle and the receptacle of young buds. B-C, Close-up of buds at stages 3 and 7, respectively, where starch accumulates at their basal part and within the peduncle and the receptacle. D, Stage 8 bud where some starch deposits develop within the stamen (arrowhead) and the basal region of the carpel (arrow). E, A flower bud at completion of the development of the four anther wall layers. Starch accumulation extends to the filament (thick arrow) and the connective tissue (thin arrow), and is still seen within the lateral wall of the carpel (arrowheads). F, During male meiosis, starch grain deposits extend to the newly formed endothecium (arrowheads). G-I, Tetrad stage of male meiosis. The first peak of starch amylogenesis in the stamen. In the carpel, starch amylogenesis switched from the lateral wall to the placenta-septum region (arrowhead). J-K, Early microspore development. J, The short stamen (*) just released microspores and is practically devoid of starch grains. The long stamen (**) have rounded microspores with a much more prominent exine. K, Starch starts to build up again in the filament (thin arrow), the connective tissue (thick arrow), and the staminal envelope (arrowheads). L-M, Bicellular stage (short stamens removed). This stage denotes the peak of the second starch wave in the staminal envelope. Pollen grains show a high starch accumulation. N-O, Late bicellular-early tricellular stage. While most of the starch grains in the staminal envelope are consumed, the pollen grains reach the peak of the unique starch wave. Starch is frequently seen surrounding the vegetative nucleus (inset in F). P-U, Successive developmental stages from the same inflorescence, illustrating the formation of large starch deposits within the sporophytic tissues of the stamen and its subsequent consumption just before anthesis. P, While a short stamen (arrowhead) is still at the end of the second wave, long stamens (arrow) have already started the third amylogenesis wave. Q, All long stamens show high starch deposition and are at the peak of the third starch accumulation wave. R-S, While a short stamen is still at the peak of its third wave, starch deposits already vanished from the anthers of long stamens. T, All stamens are at the same starch deposition stage maintaining conspicuous starch deposits in the filaments. U Anthesis: while starch vanishes progressively from the filaments, large deposits appear in the parenchyma of the style. V-Y, Starch accumulation/consumption in the anther during the third starch synthesis wave. V-W, Two optical sections illustrating strong starch accumulation in the endothecium and the connective tissue. X-Y, Two optical sections illustrating how starch disappears from the entire anther except for the stomata; pollen grains continue their amylolytic activity. Z, Mature pollen grains showing an intense PAS-positive staining; very few and small starch grains might persist (arrowheads within inset). Flower stages according to Smyth et al., 1990. Bars = 20 μm.

Figure 2. Starch turnover during ovule, and early embryo and silique development. A-C, During meiosis: megaspore mother cell (A), and functional megaspore stage (B,C) are illustrated. Starch accumulated in the placenta (thin arrow), the funiculus (arrowheads), and the chalazal region below the nucellus (thick arrows). D, Division and elongation of the embryo sac showing an extension of starch deposits to the integuments. E, Starch starts to build up in the central cell when the two polar nuclei lie next to each other (arrows). F, Strong starch accumulation in the parenchymatic cells of the style at anthesis. G-H, Ovules at anthesis (G) and during fertilization (H), showing more conspicuous starch accumulation in the central cell (surrounding the secondary endosperm nucleus, see inset within G), the distal portion of the funiculus, the micropylar portion of the integuments, and the chalazal proliferating tissue. I-L, Starch accumulation is maintained in the dividing zygote (arrow) and endosperm (arrowheads: uni-nuclear in I, bi-nuclear in J, four- or eight-nuclear in K and L). Notice the trace of a discharged pollen tube in I (thick arrow). M-P, Starch disappears from all tissues but the chalazal proliferating tissue. Notice the crushed nucellar cells (arrow) between the chalazal cyst of the endosperm and the starch-accumulating proliferating tissue in M, the pronounced ring-like shape of starch accumulation in N, the depletion of starch at the micropylar part of the seed in O, and the cells forming an inverted cup-like shape that are filled with starch and in close contact with the chalazal cyst in P. Q-R, A new wave a starch amylogenesis occurs at the octant embryo stage (Q) and is more conspicuous at the dermatogen stage (R); the endosperm is starchless. S-U, Low magnification views of different post-fertilization stages that are easily recognizable by their starch accumulation

pattern and/or intensity. Uni-nuclear (arrows) and bi-nuclear (arrowheads) endosperm stages in S; four-nuclear endosperm stages (arrows) in T; unfertilized starchless ovule (arrow), quadrant embryo (*), octant embryo (**), and dermatogen embryo stages (***) in U. Notice the persistence of starch in the style and the beginning of the basipetal starch accumulation in the silique walls and the placenta-septum region in S. V, A low magnification view of a silique illustrating the basipetal starch accumulation in the valves. W, A middle silique portion with octant and dermatogen embryos, where conspicuous starch accumulation occurs in the valves and the placenta-septum region. Bars = 20 μm.

Figure 3. The gene expression cluster during early microspore development. Co-expressed (log2-scale of expression values) sugar (A), starch (B), and sugar-phosphate (C) transport and metabolism genes during pollen development (first 4 x-axis ticks: microspore, bicellular, tricellular, and mature pollen grains), and during *in vitro* pollen tube growth (last 3 x-axis ticks: hydrated pollen grain, and 30 min and 240 min after germination).

Figure 4. Carbohydrate transport to and metabolism within the chalazal region of the seed. A, A seed at the single-cell stage of the embryo proper is shown to illustrate the two chalazal regions (chalazal seed coat in red and chalazal endosperm in blue) used in transcriptome analyses. B-E, Expression values (log2-scale) for starch synthesis (B), starch degradation (C), *GPT1* (D), and of highly expressed invertase and monosacharide transporters during early embryo development (E). Please refer to Supplemental Fig. S2 and Supplemental Fig. S3 for a full expression analysis of the 197 genes in these and other tissues, and to Table 1 for the full name of the genes.

Figure 5. Starch turnover in starch biosynthesis mutant lines. A, Strong starch accumulation in a wild-type cauline leaf at the end of the light phase. B, Starch accumulates in the peduncle (arrow) and the receptacle (arrowhead) of young wild-type buds. C, Highly reduced starch accumulation in mesophyll cells of a *pgi1-1* cauline leaf at the end of the light phase. Higher starch accumulation is, however, maintained around vascular tissues (arrow). D, Starch accumulates in the peduncle (arrow) and the receptacle (arrowhead) of young *pgi1-1* mutant buds. E-F, No starch accumulation is observed in any tissue of cauline leaves (E) or young buds (F) of the *pgm1-1* mutant at the end of the light phase. G-H, While no strong effect is observed on starch accumulation in cauline leaves (G), an appreciable reduction is seen in young *gpt1-3* buds (H) at the end of the light phase. I1-3, Different stages of *pgi1-1* stamen development illustrating that the second and third wave of starch accumulation were not affected. J1-3, *pgm1-1* stamen at different stages illustrating the absence of starch accumulation during anther development. K1-2, Unaffected second (K1) and third (K2) starch synthesis waves in *gpt1-3* stamen. L-O, Starch distribution in wild-type (L), *pgi1-1* (M), *pgm1-1* (N), and *gpt1-3* (O) flowers just before anthesis. Notice the reduced starch accumulation in *pgi1-1* sepals, the absence of starch accumulation in the whole *pgm1-1* flower, and the reduction of starch accumulation in the *gpt1-3* pistil. P, Typical starch accumulation in wild-type ovules at anthesis. Q, Highly reduced starch accumulation in *gpt1-3* ovules. Notice the absence of conspicuous starch accumulation in the central cell. R1, Close-up of starch accumulation in wild-type ovules. R2-3, Close-up of reduced (R2) or highly reduced (R3) starch accumulation in *gpt1-3* ovules. R4-5, Reduced starch accumulation in *gpt1-3* during early embryo (arrow in R4) development and in the silique valves (R5). Notice the unaffected starch accumulation in more advanced seeds. S1-S3, Unaffected starch accumulation during different stages of ovule and embryo development in *pgi1-1*. T1-T3, Absence of starch accumulation at different stages of ovule and embryo development in pgm1-1. Bars = 20 μm.

Figure 6. Digital droplet PCR analysis of *GPT1* transcript levels (A), and starch content (B) in sepals, stamen, and carpels of wild-type and *gpt1-3* flowers at opening. A, ddPCR values are means of measurements of three biological replicates normalized to 10,000 molecules of *IPP2*. B, Starch content values are means of measurements of four biological replicates. Error bars are SEM. *** denotes highly significant value ($p < 0.01$). The inset within (A) is a ddPCR analysis of *GPT1* transcript levels in single biological samples of cauline leaves and whole flowers.

591 **Figure 7**. Model of starch synthesis in pollen grains. A schematic representation of carbohydrate metabolism and
592 transport in the pollen grain. All expressed isoforms during pollen development are indicated in red. Sugar uptake by
593 the pollen occurs only via the apoplast because developing microspores are symplastically isolated. Sucrose is either
594 transported via the apoplast (SUC transporters) or metabolized first by cell wall invertases, and the resulting
595 monosaccharides transported by STP, PMT, and INT transporters. In the cytosol, expressed genes of the different
596 metabolic routes for sucrose, monosaccharide, hexose-phosphate, and starch metabolism are depicted. Not or lowly
597 expressed but important genes are indicated in green; expressed genes with unknown functions or with unknown
598 substrate specificities are in blue; and the three genes for which we analyzed insertional mutants are highlighted by red
599 boxes. Based on these expression patterns, the most likely pathway of starch biosynthesis within the developing pollen
600 grain is highlighted in yellow. Refer to Table 1 for full names of enzymes and genes.
601
602

LITERATURE CITED

Andriotis VME, Pike MJ, Bunnewell S, Hills MJ, Smith AM (2010b) The plastidial glucose-6-phosphate/phosphate antiporter GPT1 is essential for morphogenesis in *Arabidopsis* embryos. Plant J **64**: 128-139

Andriotis VME, Pike MJ, Kular B, Rawsthorne S, Smith AM (2010a) Starch turnover in developing oilseed embryos. New Phytologist **187**: 791–804

Angeles-Núñez JG, Tiessen A (2010) *Arabidopsis* sucrose synthase 2 and 3 modulate metabolic homeostasis and direct carbon towards starch synthesis in developing seeds. Planta **232**: 701–718

Bahaji A, Sanchez-Lopez AM, De Diego N, Munoz FJ, Baroja-Fernández E, Li J, Ricarte-Bermejo A, Baslam M, Aranjuelo I, Almagro G, et al (2015) Plastidic phosphoglucose isomerase is an important determinant of starch accumulation in mesophyll cells, growth, photosynthetic capacity, and biosynthesis of plastidic cytokinins in Arabidopsis. PLoS One **10**: e0119641

Baroja-Fernández E, Muñoz FJ, Bahaji A, Almagro G, Pozueta-Romero J. (2012) Letter: Reply to Smith et al.: No evidence to challenge the current paradigm on starch and cellulose biosynthesis involving sucrose synthase activity. Proc Natl Acad Sci USA **109**: E777.

Barratt DHP, Derbyshire P, Findlay K, Pike M, Wellner N, Lunn J, Feil R, Simpson C, Maule AJ, Smith AM (2009) Normal growth of *Arabidopsis* requires cytosolic invertase but not sucrose synthase. Proc Natl Acad Sci USA **106**: 13124–13129

Baud S, Boutin J, Miquel M, Lepiniec L, Rochat C (2002) An integrated overview of seed development in *Arabidopsis thaliana* ecotype WS. Plant Physiol Biochem **40**: 151–160

Belmonte MF, Kirkbride RC, Stone SL, Pelletier JM, Bui AQ, Yeung EC, Hashimoto M, Fei J, Harada CM, Munoz MD, et al. (2013) Comprehensive developmental profiles of gene activity in regions and subregions of the *Arabidopsis* seed. Proc Natl Acad Sci USA **110**: E435–E444

Boavida LC, Borges F, Becker JD, Feijó JA (2011) Whole genome analysis of gene expression reveals coordinated activation of signaling and metabolic pathways during pollen-pistil interactions in Arabidopsis. Plant Physiol **155**: 2066–2080

Borges F, Gomes G, Gardner R, Moreno N, McCormick S, Feijó JA, Becker JD (2008) Comparative transcriptomics of *Arabidopsis* sperm cells. Plant Physiol **148**: 1168-1181

Buell K (1952) Developmental morphology in *Dianthus*. II. Starch accumulation in ovule and seed. Am J Bot **39**: 458–467

Caspar T, Huber SC, Somerville C (1985) Alterations in growth, photosynthesis, and respiration in a starchless mutant of *Arabidopsis thaliana* (L.) deficient in chloroplast phosphoglucomutase activity. Plant Physiol **79**: 11–17

Chen L-Q, Hou B-H, Lalonde S, Takanaga H, Hartung ML, Qu X-Q, Guo W-J, Kim J-G, Underwood W, Chaudhuri B, et al (2010) Sugar transporters for intercellular exchange and nutrition of pathogens. Nature **468**: 527–532

Clément C, Chavant L, Burrus M, Audran JC (1994) Anther starch variations in *Lilium* during pollen development. Sex Plant Reprod **7**: 347–356

Clément C, Pacini E (2001) Anther plastids in angiosperms. Bot Rev **67**: 54–73

Crevillén P, Ballicora MA, Mérida Á, Preiss J, Romero JM (2003) The different large subunit isoforms of *Arabidopsis thaliana* ADP-glucose pyrophosphorylase confer distinct kinetic and regulatory properties to the heterotetrameric enzyme. J Biol Chem **278**: 28508–28515

Crevillén P, Ventriglia T, Pinto F, Orea A, Mérida Á, Romero JM (2005) Differential pattern of expression and sugar regulation of *Arabidopsis thaliana* ADP-glucose pyrophosphorylase-encoding genes. J Biol Chem **280**: 8143–8149

Déjardin A, Rochat C, Wuillème S, Boutin JP (1997) Contribution of sucrose synthase, ADP-glucose pyrophosphorylase and starch synthase to starch synthesis in developing pea seeds. Plant Cell Environ **20**: 1421–1430

Fallahi H, Scofield GN, Badger MR, Chow WS, Furbank RT, Ruan Y-L (2008) Localization of sucrose synthase in developing seed and siliques of *Arabidopsis thaliana* reveals diverse roles for SUS during development. J Exp Bot **59**: 3283–3295

Feijó JA, Pais MSS (1988) Ultrastructural modifications of plastids and starch metabolism during the microsporogenesis of *Ophrys lutea* (Orchidaceae). Ann Bot **61**:215-219

Fettke J, Malinova I, Albrecht T, Hejazi M, Steup M (2011) Glucose-1-phosphate transport into protoplasts and chloroplasts from leaves of *Arabidopsis*. Plant Physiol **155**: 1723–1734

Flügge U-I (1999) Phosphate translocators in plastids. Annu Rev Plant Physiol Plant Mol Biol 50:27-45.

Geigenberger P (2011) Regulation of starch biosynthesis in response to a fluctuating environment. Plant Physiology **155**: 1566–1577

Geigenberger P, Stitt M, Fernie AR (2004) Metabolic control analysis and regulation of the conversion of sucrose to starch in growing potato tubers. Plant Cell Environ **27**: 655–673

Guan YF, Huang XY, Zhu J, Gao JF, Zhang HX, Yang ZN (2008) RUPTURED POLLEN GRAIN1, a member of the MtN3/ saliva gene family, is crucial for exine pattern formation and cell integrity of microspores in Arabidopsis. Plant Physiol **147**: 852–863

Herr JM Jr (1971) A new clearing-squash technique for the study of ovule development in angiosperms. Am J Bot **58**: 785–790

Herr JM Jr (1972) Applications of a new clearing technique for the investigation of vascular plant morphology. J. Elisha Mitchell Sci. Soc. **88**:137-43.

Honys D, Twell D (2004) Transcriptome analysis of haploid male gametophyte development in *Arabidopsis*. Genome Biol. **5**:

Hostettler C, Kölling K, Santelia D, Streb S, Kötting O, Zeeman SC (2011). Analysis of starch metabolism in chloroplasts. Methods Mol Biol **775**: 387-410.

Irizarry RA, Bolstad BM, Collin F, Cope LM, Hobbs, B, Speed TP (2003) Summaries of Affymetrix GeneChip probe level data. Nucleic Acids Res. **31**: e15

Kammerer B, Fischer K, Hilpert B, Schubert S, Gutensohn M, Weber A, Flügge UI (1998) Molecular characterization of a carbon transporter in plastids from heterotrophic tissues: the glucose 6-phosphate/phosphate antiporter. Plant Cell **10**: 105–117

Kram BW, Xu WW, Carter CJ (2009) Uncovering the *Arabidopsis thaliana* nectary transcriptome: investigation of differential gene expression in floral nectariferous tissues. BMC Plant Biol **9**: 92

Kunz HH, Häusler RE, Fettke J, Herbst K, Niewiadomski P, Gierth M, Bell K, Steup M, Flügge UI, Schneider A (2010) The role of plastidial glucose-6-phosphate/phosphate translocators in vegetative tissues of *Arabidopsis thaliana* mutants impaired in starch biosynthesis. Plant Biology **12**: 115–128

Mansfield SG, Briarty LG (1991) Early embryogenesis in *Arabidopsis thaliana*. II. The developing embryo. Can J Bot **69**: 461–476

Miki-Hiroshige H, Nakamura S (1983) Growth and differentiation of amyloplasts during male gamete development in *Lilium longiflorum*. In: Mulcahy DL, Ottaviano E (eds) Pollen: biology and implications for plant breeding. Elsevier, Amsterdam, pp 141-147

Muñoz FJ, Baroja-Fernández E, Moran-Zorzano MT, Viale AM, Etxeberria E, Alonso-Casajus N, Pozueta-Romero J (2005) Sucrose synthase controls both intracellular ADP glucose levels and transitory starch biosynthesis in source leaves. Plant Cell Physiol **46**: 1366–1376.

Nguyen H, Brown RC, Lemmon BE (2000) The specialized chalazal endosperm in *Arabidopsis thaliana* and *Lepidium virginicum* (Brassicaceae). Protoplasma **212**: 99–110

Niewiadomski P, Knappe S, Geimer S, Fischer K, Schulz B, Unte US, Rosso MG, Ache P, Flügge UI, Schneider A (2005) The *Arabidopsis* plastidic glucose 6-phosphate/phosphate translocator GPT1 is essential for pollen maturation and embryo sac development. Plant Cell 17: 760–775

Pacini E, Franchi GG (1983) Pollen grain development in *Smilax aspersa* L. and possible function of the loculus. In: Mulcahy DL, Ottaviano E (eds) Pollen: biology and implications for plant breeding. Elsevier, Amsterdam, pp 183-190

Park SK, Howden R, Twell D (1998) The *Arabidopsis thaliana* gametophytic mutation *gemini pollen1* disrupts microspore polarity, division asymmetry and pollen cell fate. Development **125**: 3789-3799

Pina P, Pinto F, Feijó JA, Becker JD (2005) Gene family analysis of the Arabidopsis pollen transcriptome reveals biological implications for cell growth, division control, and gene expression regulation. Plant Physiol **138**: 744-756

Qin Y, Leydon AR, Manziello A, Pandey R, Mount D, Denic S, Vasic B, Johnson MA, Palanivelu R (2009) Penetration of the stigma and style elicits a novel transcriptome in pollen tubes, pointing to genes critical for growth in a pistil. PLoS Genet **5**: e1000621

Reznickova SA, Willemse MTM (1980) Formation of pollen in the anther of *Lilium*. II. The function of the surrounding tissues in the formation of pollen and pollen wall. Acta Bot Neerl **29**: 141-156

Rolletschek H, Nguyen TH, Häusler RE, Rutten T, Göbel C, Feussner I, Radchuk R, Tewes A, Claus B, Klukas C, Linemann U, Weber H, Wobus U, Borisjuk L (2007) Anti-sense inhibition of the plastidial glucose-6-phosphate / phosphate translocator in *Vicia* seeds shifts cellular differentiation and promotes protein storage. Plant Journal, 51, 468–484.

Schmid M, Davison TS, Henz SR, Pape UJ, Demar M, Vingron M, Schölkopf B, Weigel D, Lohmann J (2005) A gene expression map of *Arabidopsis* development. Nature Genet **37**: 501-506

Schmid MW, Schmidt A, Grossniklaus U (2015) The female gametophyte: an emerging model for cell type-specific systems biology in plant development. Front Plant Sci. **6**: 907.

Schmidt A, Wüest SE, Vijverberg K, Baroux C, Kleen D, Grossniklaus U (2011) Transcriptome analysis of the *Arabidopsis* megaspore mother cell uncovers the importance of RNA helicases for plant germline development. PLoS Biol **9**: e1001155

Schulz SP, Jensen WA (1969) *Capsella* embryogenesis: the suspensor and the basal cell. Protoplasma **67**: 139-163.

Schulz SP, Jensen WA (1971) *Capsella* embryogenesis: the chalazal proliferating tissue. J Cell Sci **8**: 201–227

Smith AM (2012) Starch in the Arabidopsis plant. Starch/Stärke 64: 421–434

Smith AM, Kruger NJ, Lunn JE (2012) Letter: Source of sugar nucleotides for starch and cellulose synthesis. Proc Natl Acad Sci USA **109**: E77

Smyth DR, Bowman JL, Meyerowitz EM (1990) Early flower development in *Arabidopsis*. Plant Cell **2**: 755-767

Streb S, Egli B, Eicke S, Zeeman SC (2009) The debate on the pathway of starch synthesis: a closer look at low-starch mutants lacking plastidial phosphoglucomutase supports the chloroplast-localized pathway. Plant Physiol **151**: 1769–1772

Streb S, Zeeman SC (2012) Starch metabolism in *Arabidopsis*. Arabidopsis Book. doi: 10.1199/tab.0160

Truernit E, Stadler R, Baier K, Sauer N (1999) A male gametophyte-specific monosaccharide transporter in *Arabidopsis*. Plant J **17**: 191–201

Tsai H-L, Lue W-L, Lu K-J, Hsieh M-H, Wang S-M, Chen J (2009) Starch synthesis in Arabidopsis is achieved by spatial cotranscription of core starch metabolism genes. Plant Physiol **151**: 1582–1595

Wang L, Ruan YL (2012) New insights into roles of cell wall invertase in early seed development revealed by comprehensive spatial and temporal expression patterns of *GhCWIN1* in cotton. Plant Physiol **160**: 777–787

Wang Y, Zhang W-Z, Song L-F, Zou J-J, Su Z, Wu W-H (2008) Transcriptome analyses show changes in gene expression to accompany pollen germination and tube growth in Arabidopsis. Plant Physiol **148**: 1201–1211

Weigel D, Glazebrook J (2002) *Arabidopsis*: a laboratory manual. Cold Spring Harbor Laboratory Press, Cold Spring Harbor, New York

Figure 1. The three starch synthesis waves in the stamen envelope. A-J first wave, J-O second wave, and P-Z third wave. A, Starch accumulates within the peduncle and the receptacle of young buds. B-C, Close-up of buds at stages 3 and 7, respectively, where starch accumulates at their basal part and within the peduncle and the receptacle. D, Stage 8 bud where some starch deposits develop within the stamen (arrowhead) and the basal region of the carpel (arrow). E, A flower bud at completion of the development of the four anther wall layers. Starch accumulation extends to the filament (thick arrow) and the connective tissue (thin arrow), and is still seen within the lateral wall of the carpel (arrowheads). F, During male meiosis, starch grain deposits extend to the newly formed endothecium (arrowheads). G-I, Tetrad stage of male meiosis. The first peak of starch amylogenesis in the stamen. In the carpel, starch amylogenesis switched from the lateral wall to the placenta-septum region (arrowhead). J-K, Early microspore development. J, The short stamen (*) just released microspores and is practically devoid of starch grains. The long stamen (**) have rounded microspores with a much more prominent exine. K, Starch starts to build up again in the filament (thin arrow), the connective tissue (thick arrow), and the staminal envelope (arrowheads). L-M, Bicellular stage (short stamens removed). This stage denotes the peak of the second starch wave in the staminal envelope. Pollen grains show a high starch accumulation. N-O, Late bicellular-early tricellular stage. While most of the starch grains in the staminal envelope are consumed, the pollen grains reach the peak of the unique starch wave. Starch is frequently seen surrounding the vegetative nucleus (inset in F). P-U, Successive developmental stages from the same inflorescence, illustrating the formation of large starch deposits within the sporophytic tissues of the stamen and its subsequent consumption just before anthesis. P, While a short stamen (arrowhead) is still at the end of the second wave, long stamens (arrow) have already started the third amylogenesis wave. Q, All long stamens show high starch deposition and are at the peak of the third starch accumulation wave. R-S, While a short stamen is still at the peak of its third wave, starch deposits already vanished from the anthers of long stamens. T, All stamens are at the same starch deposition stage maintaining conspicuous starch deposits in the filaments. U Anthesis: while starch vanishes progressively from the filaments, large deposits appear in the parenchyma of the style. V-Y, Starch accumulation/consumption in the anther during the third starch synthesis wave. V-W, Two optical sections illustrating strong starch accumulation in the endothecium and the connective tissue. X-Y, Two optical sections illustrating how starch disappears from the entire anther except for the stomata; pollen grains continue their amylolytic activity. Z, Mature pollen grains showing an intense PAS-positive staining; very few and small starch grains might persist (arrowheads within inset). Flower stages according to Smyth et al. 1990. Bars = 20 μm.

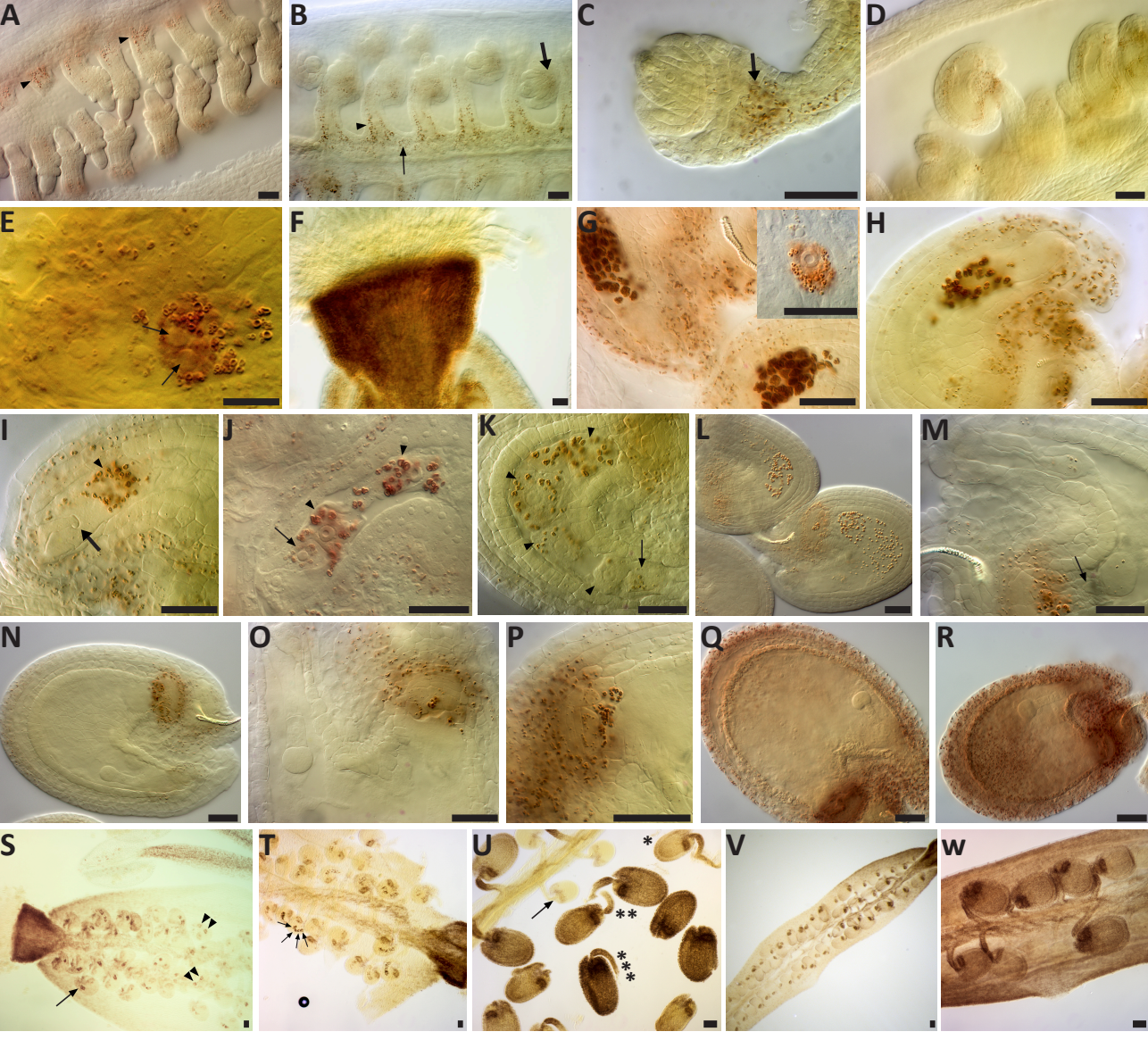

Figure 2. Starch turnover during ovule, and early embryo and silique development. A-C, During meiosis: megaspore mother cell (A), and functional megaspore stage (B,C) are illustrated. Starch accumulated in the placenta (thin arrow), the funiculus (arrowheads), and the chalazal region below the nucellus (thick arrows). D, Division and elongation of the embryo sac showing an extension of starch deposits to the integuments. E, Starch starts to build up in the central cell when the two polar nuclei lie next to each other (arrows). F, Strong starch accumulation in the parenchymatic cells of the style at anthesis. G-H, Ovules at anthesis (G) and during fertilization (H), showing more conspicuous starch accumulation in the central cell (surrounding the secondary endosperm nucleus, see inset within G), the distal portion of the funiculus, the micropylar portion of the integuments, and the chalazal proliferating tissue. I-L, Starch accumulation is maintained in the dividing zygote (arrow) and endosperm (arrowheads: uni-nuclear in I, bi-nuclear in J, four- or eight-nuclear in K and L). Notice the trace of a discharged pollen tube in I (thick arrow). M-P, Starch disappears from all tissues but the chalazal proliferating tissue. Notice the crushed nucellar cells (arrow) between the chalazal cyst of the endosperm and the starch-accumulating proliferating tissue in M, the pronounced ring-like shape of starch accumulation in N, the depletion of starch at the micropylar part of the seed in O, and the cells forming an inverted cup-like shape that are filled with starch and in close contact with the chalazal cyst in P. Q-R, A new wave a starch amylogenesis occurs at the octant embryo stage (Q) and is more conspicuous at the dermatogen stage (R); the endosperm is starchless. S-U, Low magnification views of different post-fertilization stages that are easily recognizable by their starch accumulation pattern and/or intensity. Uni-nuclear (arrows) and bi-nuclear (arrowheads) endosperm stages in S; four-nuclear endosperm stages (arrows) in T; unfertilized starchless ovule (arrow), quadrant embryo (*), octant embryo (**), and dermatogen embryo stages (***) in U. Notice the persistence of starch in the style and the beginning of the basipetal starch accumulation in the silique walls and the placenta-septum region in S. V, A low magnification view of a silique illustrating the basipetal starch accumulation in the valves. W, A middle silique portion with octant and dermatogen embryos, where conspicuous starch accumulation occurs in the valves and the placenta-septum region. Bars = 20 μm.

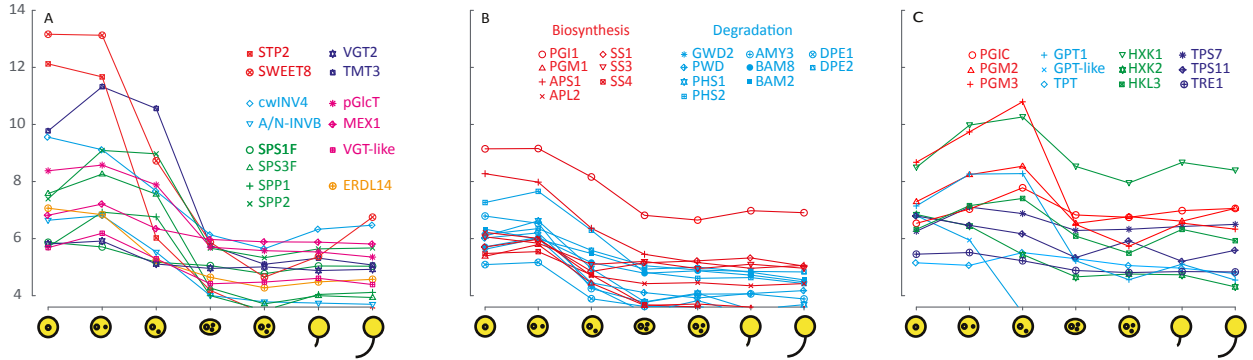

Figure 3. Gene expression clusters during early microspore development. Co-expressed (log2-scale of expression values) sugar (A), starch (B), and sugar-phosphate (C) transport and metabolism genes during pollen development (first 4 x-axis ticks: microspore, bicellular, tricellular, and mature pollen grains), and during in vitro pollen tube growth (last 3 x-axis ticks: hydrated pollen grain, and 30 min and 240 min after germination).

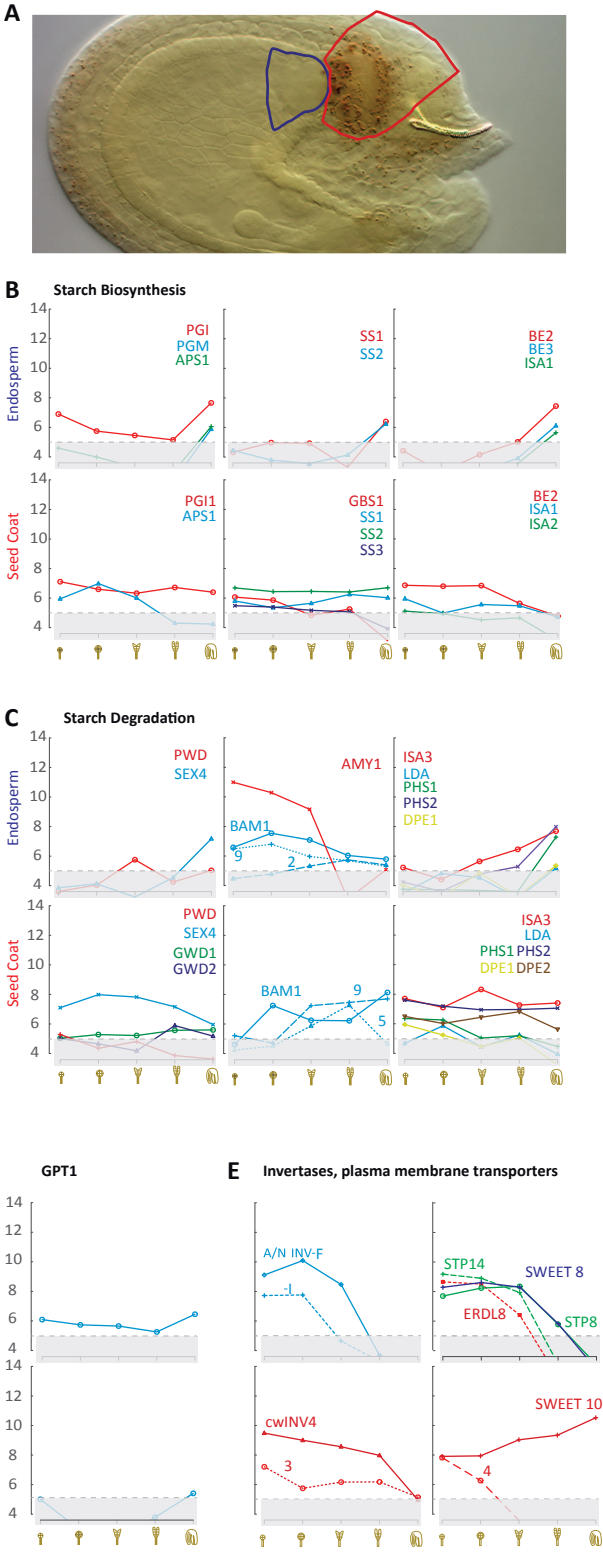

Figure 4. Carbohydrate transport to and metabolism within the chalazal region of the seed. A, A seed at the single-cell stage of the embryo proper is shown to illustrate the two chalazal regions (chalazal seed coat in red and chalazal endosperm in blue) used in transcriptome analyses. B-E, Expression values (log2-scale) for starch synthesis (B), starch degradation (C), GPT1 (D), and of highly expressed invertase and monosacharide transporters during early embryo development (E). Please refer to Supplemental Fig. S2 and Supplemental Fig. S3 for a full expression analysis of the 197 genes in these and other tissues, and to Table 1 for the full name of the genes.

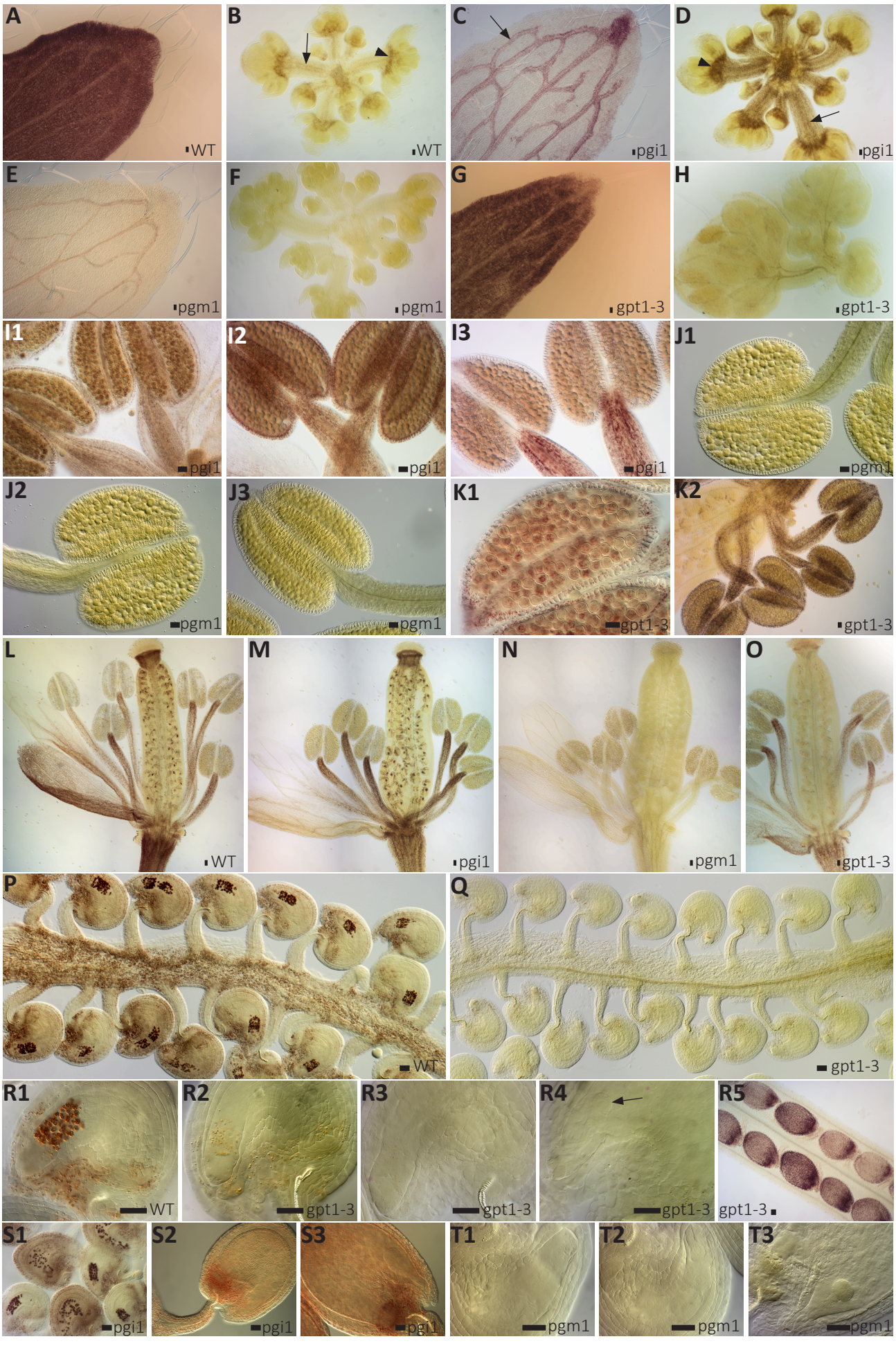
A
WT
B
WT
C
pgi1
D
pgi1
E
pgm1
F
pgm1
G
gpt1-3
H
gpt1-3
I1
pgi1
I2
pgi1
I3
pgi1
J1
pgm1
J2
pgm1
J3
pgm1
K1
gpt1-3
K2
gpt1-3
L
WT
M
pgi1
N
pgm1
O
gpt1-3
P
WT
Q
gpt1-3
R1
WT
R2
gpt1-3
R3
gpt1-3
R4
gpt1-3
R5
gpt1-3
S1
pgi1
S2
pgi1
S3
pgi1
T1
pgm1
T2
pgm1
T3
pgm1

Figure 5. Starch turnover in starch biosynthesis mutant lines. A, Strong starch accumulation in a wild-type cauline leaf at the end of the light phase. B, Starch accumulates in the peduncle (arrow) and the receptacle (arrowhead) of young wild-type buds. C, Highly reduced starch accumulation in mesophyll cells of a *pgi1-1* cauline leaf at the end of the light phase. Higher starch accumulation is, however, maintained around vascular tissues (arrow). D, Starch accumulates in the peduncle (arrow) and the receptacle (arrowhead) of young *pgi1-1* mutant buds. E-F, No starch accumulation is observed in any tissue of cauline leaves (E) or young buds (F) of the *pgm1-1* mutant at the end of the light phase. G-H, While no strong effect is observed on starch accumulation in cauline leaves (G), an appreciable reduction is seen in young *gpt1-3* buds (H) at the end of the light phase. I1-3, Different stages of *pgi1-1* stamen development illustrating that the second and third wave of starch accumulation were not affected. J1-3, *pgm1-1* stamen at different stages illustrating the absence of starch accumulation during anther development. K1-2, Unaffected second (K1) and third (K2) starch synthesis waves in *gpt1-3* stamen. L-O, Starch distribution in wild-type (L), *pgi1-1* (M), *pgm1-1* (N), and *gpt1-3* (O) flowers just before anthesis. Notice the reduced starch accumulation in *pgi1-1* sepals, the absence of starch accumulation in the whole *pgm1-1* flower, and the reduction of starch accumulation in the *gpt1-3* pistil. P, Typical starch accumulation in wild-type ovules at anthesis. Q, Highly reduced starch accumulation in *gpt1-3* ovules. Notice the absence of conspicuous starch accumulation in the central cell. R1, Close-up of starch accumulation in wild-type ovules. R2-3, Close-up of reduced (R2) or highly reduced (R3) starch accumulation in *gpt1-3* ovules. R4-5, Reduced starch accumulation in *gpt1-3* during early embryo (arrow in R4) development and in the silique valves (R5). Notice the unaffected starch accumulation in more advanced seeds. S1-S3, Unaffected starch accumulation during different stages of ovule and embryo development in *pgi1-1*. T1-T3, Absence of starch accumulation at different stages of ovule and embryo development in pgm1-1. Bars = 20 μm.

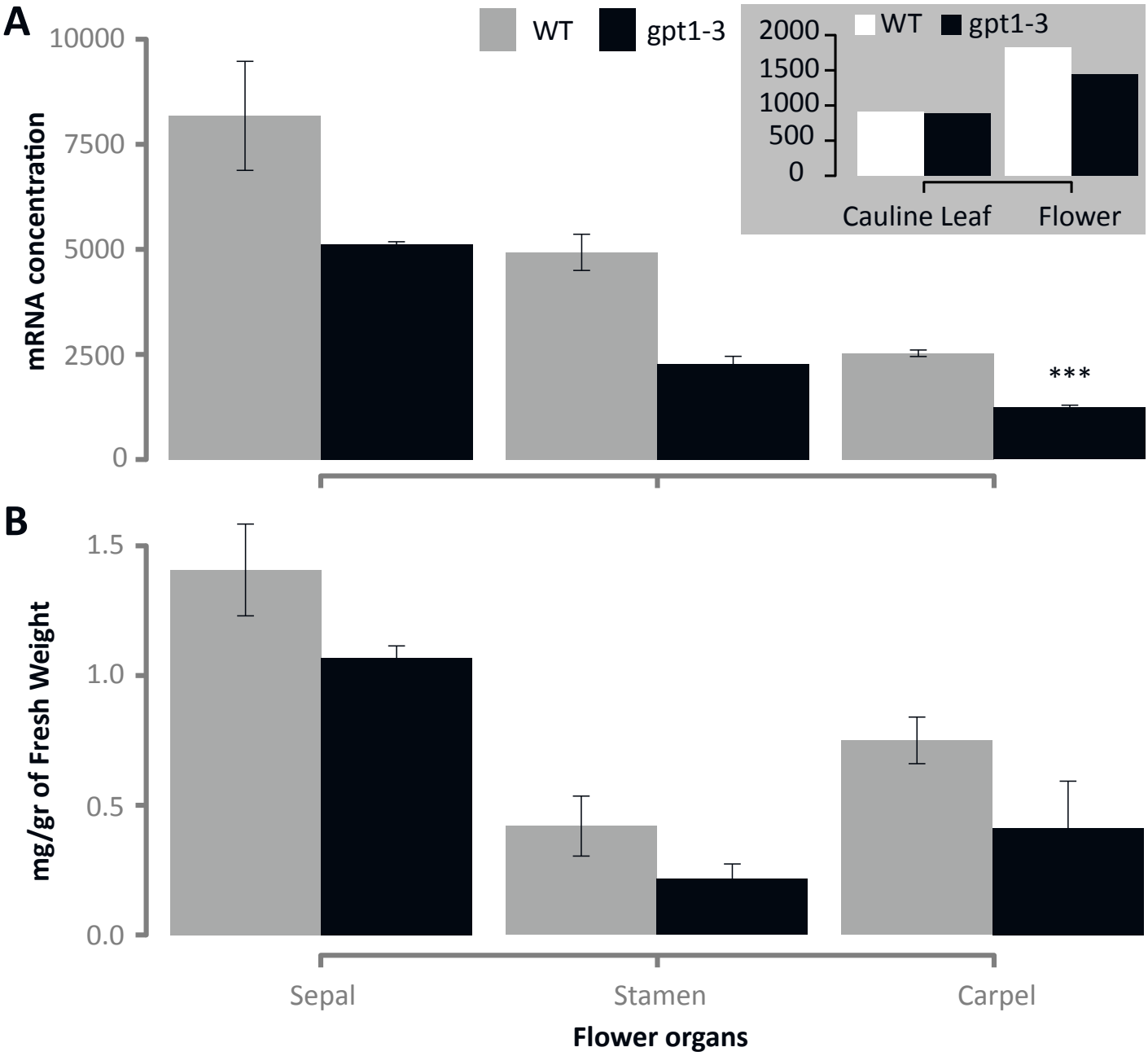

Figure 6. Digital droplet PCR analysis of GPT1 transcript levels (A), and starch content (B) in sepals, stamen, and carpels of wild-type and gpt1-3 flowers at opening. A, ddPCR values are means of measurements of three biological replicates normalized to 10,000 molecules of IPP2. B, Starch content values are means of measurements of four biological replicates. Error bars are SEM. *** denotes highly significant value ($p < 0.01$). The inset within (A) is a ddPCR analysis of GPT1 transcript levels in single biological samples of cauline leaves and whole flowers.

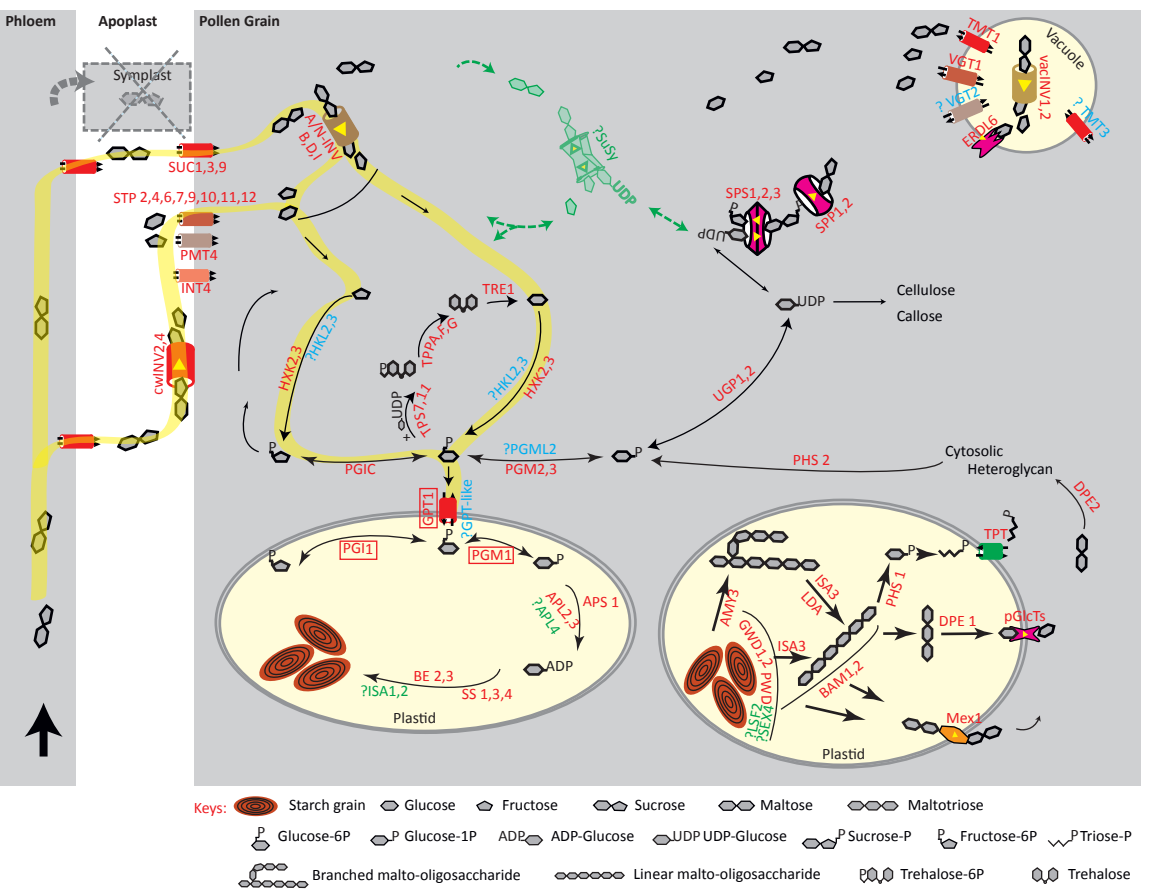

Figure 7. Model of starch synthesis in pollen grains. A schematic representation of carbohydrate metabolism and transport in the pollen grain. All expressed isoforms during pollen development are indicated in red. Sugar uptake by the pollen occurs only via the apoplast because developing microspores are symplastically isolated. Sucrose is either transported via the apoplast (SUC transporters) or metabolized first by cell wall invertases, and the resulting monosaccharides transported by STP, PMT, and INT transporters. In the cytosol, expressed genes of the different metabolic routes for sucrose, monosaccharide, hexose-phosphate, and starch metabolism are depicted. Not or lowly expressed but important genes are indicated in green; expressed genes with unknown functions or with unknown substrate specificities are in blue; and the three genes for which we analyzed insertional mutants are highlighted by red boxes. Based on these expression patterns, the most likely pathway of starch biosynthesis within the developing pollen grain is highlighted in yellow. Refer to Table 1 for full names of enzymes and genes.

Wuest SE, Vijverberg K, Schmidt A, Weiss M, Gheyselinck J, Lohr M, Wellmer F, Rahnenführer J, Mering C, Grossniklaus U (2010) *Arabidopsis* female gametophyte gene expression map reveals similarities between plant and animal gametes. Curr Biol **20**: 506–512

Yu HJ, Hogan P, Sundaresan V (2005) Analysis of the female gametophyte transcriptome of *Arabidopsis* by comparative expression profiling. Plant Physiol **139**: 1853–1869

Yu TS, Lue WL, Wang SM, Chen J (2000) Mutation of Arabidopsis plastid phosphoglucose isomerase affects leaf starch synthesis and floral initiation. Plant Physiol **123**: 319–325

Zhang L, Häusler RE, GreitenC, Hajirezaei MR, Haferkamp Neuhaus HEI, Flügge UI, Ludewig F (2008) Overriding the co-limiting import of carbon and energy into tuber amyloplasts increases the starch content and yield of transgenic potato plants. Plant Biotechnology Journal, 6, 453–464.